Pergamon

Int. J. Heat Mass Transfer. Vol. 37, No. 16, pp. 2505–2516, 1994

0017-9310/94 $7.00 + 0.00

0017-9310(94)E0085-9

A simulation for multiple moving boundaries during melting inside an enclosure imposed with cyclic wall temperature

C. J. HO and C. H. CHU

Department of Mechanical Engineering, National Cheng Kung University, Tainan, Taiwan 70101, R.O.C.

(*Received* 8 *November* 1993 *and in final form* 24 *February* 1994)

Abstract—The focus of the present study is the numerical simulation of multiple moving solid–liquid interfaces during natural-convection-dominated melting of a pure material contained in a vertical square enclosure imposed with time-periodic large-amplitude oscillatory wall temperature. A solution algorithm extended from the method developed in a previous study is used and demonstrated to be capable of tracking the multiple moving boundaries due to the time-periodic large-amplitude wall-temperature oscillation crossing the fusion point of the phase-change medium confined in the enclosure. The numerical results unveil interesting re-solidification and/or re-melting phenomena in accordance with the wall-temperature oscillation. There may coexist three solid–liquid interfaces during the sustained periodic solid–liquid phase-change process inside the enclosure. Accordingly, a complicated cyclic variation of the melting rate and the heat transfer characteristics arises as a result of the periodic occurrence of multiple moving boundaries inside the enclosure.

INTRODUCTION

OVER the past few decades, the heat transfer problem involved in solid–liquid phase-change processes (melting/freezing) has been of great research interest due to its relevance to many technological applications such as latent-heat energy storage systems, casting and crystal-growth processes, latent-heat thermal control devices, to name a few. For a comprehensive discussion of the recent advances concerning the solid–liquid phase change heat transfer problem we refer to refs. [1–4], where a large quantity of literature is mentioned and not repeated here.

In this paper we present a numerical simulation of multiple moving boundaries arising in the natural-convection-dominated melting process of a pure solid–liquid phase-change material (PCM) from a vertical wall of a square enclosure, as illustrated schematically in Fig. 1, subjected to a temporally cyclic large-amplitude wall-temperature perturbation. The present study is a follow-up to our earlier works [5, 6] in which an identical physical configuration was considered but with the sinusoidal oscillation amplitude of the hot-wall temperature limited such that the oscillatory wall temperature remained above the fusion point of the PCM. The work reported here represents a continuing effort to relax the above-mentioned restriction on the imposed amplitude of the wall-temperature perturbation such that the oscillatory wall temperature may pass through (lower and then higher than) the fusion point of the PCM, therefore giving rise to phenomena of re-freezing and then re-melting of the PCM at the wall. As a result, multiple solid–liquid interfaces may emerge during the periodic melting process inside the enclosure. With the exception of recent works of Hsieh and Choi [7, 8], it appears that there exists little or no previous work analyzing the multiple moving boundary problem induced by a time-variant thermal boundary condition. In refs. [7, 8], a unified approach based on a source and sink method was developed for the analysis of a diffusion-dominated solid–liquid phase-

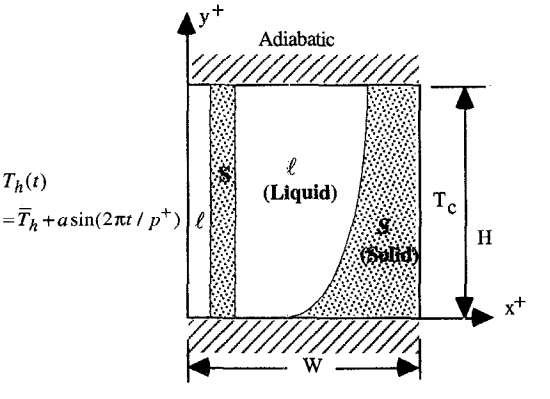

FIG. 1. Schematic diagram of the physical configuration and coordinate system.

NOMENCLATURE

a	amplitude of oscillatory surface temperature
A	dimensionless amplitude of oscillatory surface temperature, $a/(\bar{T}_h - T_f)$
c_p	specific heat
Fo	Fourier number, $\alpha_l t/H^2$
g	gravitational acceleration
H	height of enclosure
k	thermal conductivity
L	latent heat
p^+	time period
p	dimensionless time period, $\alpha_l p^+/H^2$
Pr	Prandtl number, ν_l/α_l
$\bar{q}$	average heat flux at vertical wall
Q	dimensionless heat transfer rate
Ra	Rayleigh number, $g\beta(\bar{T}_h - T_f)H^3/(\nu_l\alpha_l)$
S	dimensionless position of solid–liquid interface
Sc	subcooling factor, $(T_f - T_c)/(\bar{T}_h - T_f)$
Ste	Stefan number, $c_{p,l}(\bar{T}_h - T_f)/L$
t	time
T	temperature
V_m	volume of liquid phase-change material (PCM)
V_0	total volume of PCM
V^*	volumetric fraction of liquid PCM, V_m/V_0
W	width of enclosure
x^+, y^+	Cartesian coordinates
x, y	dimensionless coordinates, x^+/H, y^+/H.

Greek symbols

α	thermal diffusivity, $k/(\rho c_p)$
θ	dimensionless temperature, $(T - T_f)/(\bar{T}_h - T_f)$
ν	kinematic viscosity
ρ	density
ψ^+	stream function
ψ	dimensionless stream function, ψ^+/α_l
ω^+	vorticity
ω	dimensionless vorticity, $\omega^+ H^2/\alpha_l$.

Subscripts

c	cold surface
f	fusion point
h	hot surface
l	liquid phase
s	solid phase.

Superscripts

$\bar{}$	average value.

change process of a semi-infinite medium (Stefan problem) imposed with time-variant temperature and flux boundary conditions.

MATHEMATICAL FORMULATION

The physical configuration of the melting heat transfer problem under consideration is schematically illustrated in Fig. 1. The PCM contained in the square enclosure ($H = W$) is assumed to be initially at a uniform temperature T_c ($< T_f$). At a certain instant, $t = 0$, the left vertical wall of the enclosure is suddenly imposed with a temporally sinusoidal temperature perturbation of period p^+ and amplitude a about a mean value of $\bar{T}_h$; while the right vertical wall is maintained as an isothermal surface at T_c. The horizontal walls of the enclosure are assumed to be insulated thermally. For the time-periodic natural-convection-dominated melting process considered here, the dimensionless governing differential equations for the conservation of mass, momentum and energy can be formulated in terms of vorticity, stream function, and temperature as follows [6].

In the liquid region

$$\frac{\partial w}{\partial Fo} + \frac{\partial \psi}{\partial y}\frac{\partial \omega}{\partial x} - \frac{\partial \psi}{\partial x}\frac{\partial w}{\partial y} = Pr\nabla^2\omega + Pr\,Ra\frac{\partial \theta}{\partial x} \quad (1)$$

$$\nabla^2\psi = -\omega \quad (2)$$

$$\frac{\partial \theta}{\partial Fo} + \frac{\partial \psi}{\partial y}\frac{\partial \theta}{\partial x} - \frac{\partial \psi}{\partial x}\frac{\partial \theta}{\partial y} = \nabla^2\theta. \quad (3)$$

In the solid region

$$\frac{\partial \theta}{\partial Fo} = \left(\frac{\alpha_s}{\alpha_l}\right)\nabla^2\theta. \quad (4)$$

In the foregoing, the thermophysical properties of solid/liquid PCM are assumed to be independent of temperature; and the buoyancy-driven flow in the liquid PCM region is two-dimensional and laminar, adhering to the Boussinesq approximation. Moreover, the volume change associated with solid–liquid phase change and viscous dissipation are neglected. The dimensionless initial/boundary conditions for the problem are:

at $Fo = 0$;

$$\psi = \omega = 0; \quad \theta = -Sc \quad (5)$$

and for $Fo > 0$

$$y = 0 \text{ or } 1, \quad \psi = \frac{\partial \theta}{\partial y} = 0 \quad (6a)$$

$$x = 0, \quad \psi = 0, \quad \theta = 1 + A \sin\left(\frac{2\pi Fo}{p}\right) \tag{6b}$$

$$x = 1, \quad \psi = \theta = 0 \tag{6c}$$

and at the solid–liquid interface, the energy balance equation is of the form

$$\left[1 + \left(\frac{\partial S}{\partial y}\right)^2\right]\left[\left(\frac{k_s}{k_l}\right)\frac{\partial \theta}{\partial x}\bigg|_s - \frac{\partial \theta}{\partial x}\bigg|_l\right] = \frac{1}{Ste}\frac{\partial S}{\partial Fo}. \tag{6d}$$

Moreover, the average heat transfer rates at the left and right thermally active walls of the enclosure are expressed as the dimensionless heat fluxes of the following forms, respectively:

$$\bar{Q}_h = \int_0^1 \frac{\partial \theta}{\partial x}\bigg|_{x=0} dy = \frac{\bar{q}_h H}{k_l(\bar{T}_h - T_f)} \tag{7a}$$

and

$$\bar{Q}_c = \int_0^1 \frac{\partial \theta}{\partial x}\bigg|_{x=1} dy = \frac{\bar{q}_c H}{k_s(\bar{T}_h - T_f)}. \tag{7b}$$

SOLUTION METHOD

Numerical solutions of the model equations of the problem were obtained through a finite-difference method. The numerical discretization schemes adopted here basically follow those dscribed in earlier work [6]. The convective terms were approximated using the second-upwind scheme [9], while second-order central differencing was employed for the diffusion terms. The initial position of the melting front was located following the enthalpy formulation employed in earlier work [5]. As can be seen in the foregoing formulation, the time-variant left wall temperature during the second half cycle of the oscillation can be lower and then higher than the fusion point of the PCM, therefore giving rise to a phenomenon of re-freezing and then re-melting from the wall, if the dimensionless temperature oscillation amplitude is greater than unity ($A > 1$). It follows that multiple solid–liquid interfaces may coexist inside the enclosure. For the sinusoidal wall-temperature oscillation considered in the present work, there may coexist at most three solid–liquid interfaces dividing the confined PCM into four regions, as exemplified schematically in Fig. 1, such that a solid PCM layer is sandwiched between two molten PCM regions. To effectively treat the resulting multiple moving boundaries, a solution procedure extended from the method of earlier work [6] was employed. The enthalpy formulation [5] was adopted to identify and locate a newly formed solid–liquid interface that may emerge in accordance with the sinusoidal oscillation of the wall temperature. Thereafter, as the solid–liquid phase-change process progressed, the existent moving boundaries inside the enclosure were calculated explicitly using the energy balance equation, (6d). Once the locations of the moving boundaries were determined, calculations for the temperature and flow fields across the enclosure were treated implicitly. Moreover, whenever the width of the solid layer sandwiched between the liquid regions was smaller than the horizongal grid size, the solid PCM layer was treated as isothermal at the fusion temperature.

The transient solution to the problem considered was obtained using a line by line relaxation method within each time step. The implicit iteration calculations continued until a relative convergence criterion of 10^{-4} was satisfied for each field variable (stream function, vorticity, and temperature) of the problem. As a result of a series of numerical accuracy tests for convergence with mesh-size and time-step, a uniform grid system of 41×41 and a time-step of 1.25×10^{-3} were found to be adequate for the present calculation. Furthermore, the present numerical algorithm treating the multiple moving boundaries was validated by performing calculations for a conduction-dominated melting and solidification problem of a semi-infinite aluminum subjected to a time-dependent sinusoidal surface temperature [7]. As exemplified in Fig. 2, a good agreement between the prediction using the present algorithm for the multiple moving boundaries and the results of [7] was clearly obtained for the time-variant locations of the coexistent melting and freezing fronts due to the cyclic wall-temperature condition.

RESULTS AND DISCUSSION

Numerical simulations of the natural-convection-dominated melting process were undertaken for *n*-octadecane as the PCM filled in the square enclosure imposed with a time-dependent sinusoidal hot-wall-temperature condition. A total of ten simulations has been carried out with the relevant parameters in the following ranges: $A = 0.0$ to 1.5; $p = 0.25$ to 2.0; $Ra = 10^4$ to 10^5; $Ste = 0.1$, and $Sc = 0.5$. A comprehensive parametric simulation for the relevant parameters of the present problem was not attempted in

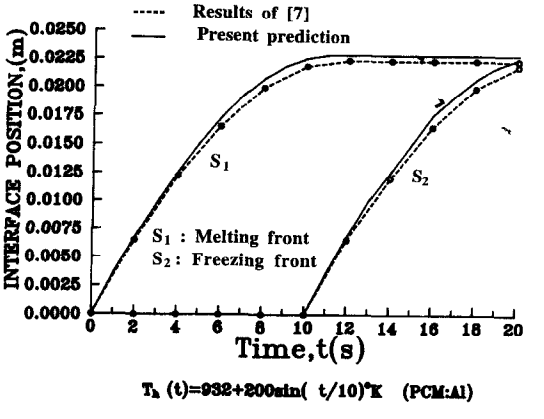

FIG. 2. Comparison of the predicted interface locations for a Stefan problem subjected to an oscillatory temperature with the results of ref. [7].

this work. The results to be presented will mainly focus on the effect of the large-amplitude ($A > 1$) cyclic wall-temperature condition on the melting process and its heat transfer characteristics inside the enclosure.

Similar to that observed in earlier works [5, 6] under a cyclic temperature perturbation while keeping the amplitude less than unity ($A < 1$), the melting process inside the *n*-octadecane-filled enclosure imposed with large-amplitude ($A > 1$) hot-wall-temperature oscillation is found to evolve towards a sustained synchronous oscillatory variation with time following a transient oscillatory regime. Furthermore, as exemplified in Fig. 3, the steady periodic variation of the volumetric melting fraction (V^*) and the dimensionless average heat transfer rates ($\bar{Q}_h$ and $\bar{Q}_c$) at the hot and cold walls of the enclosure for $A > 1$ behaves considerably differently than for $A < 1$. To have a close-up look of the difference in the cyclic variation between $A > 1$ and $A < 1$, Fig. 4(a) magnifies the temporal variation of V^* and $\bar{Q}_h$ for three different temperature perturbation amplitudes $A = 0.75$, 1.1 and 1.5 over the sixteenth cycle of the periodic melting process shown in Fig. 3, together with the corresponding cyclic variation of the dimensionless hot-wall temperature in Fig. 4(b). It can be clearly seen in Fig. 4(a) that contrary to the smooth cyclic variation

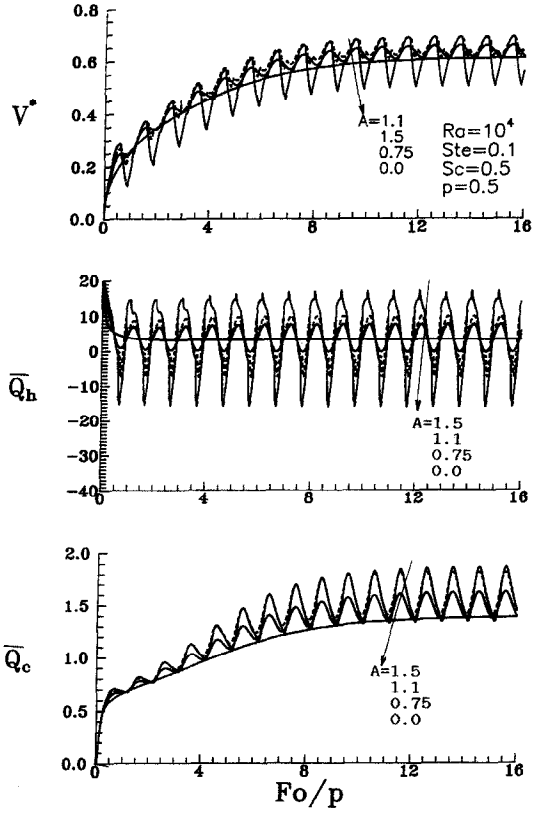

FIG. 3. Temporal variation of melting fraction and average heat transfer rates at the vertical walls of the enclosure imposed with a large-amplitude wall-temperature oscillation.

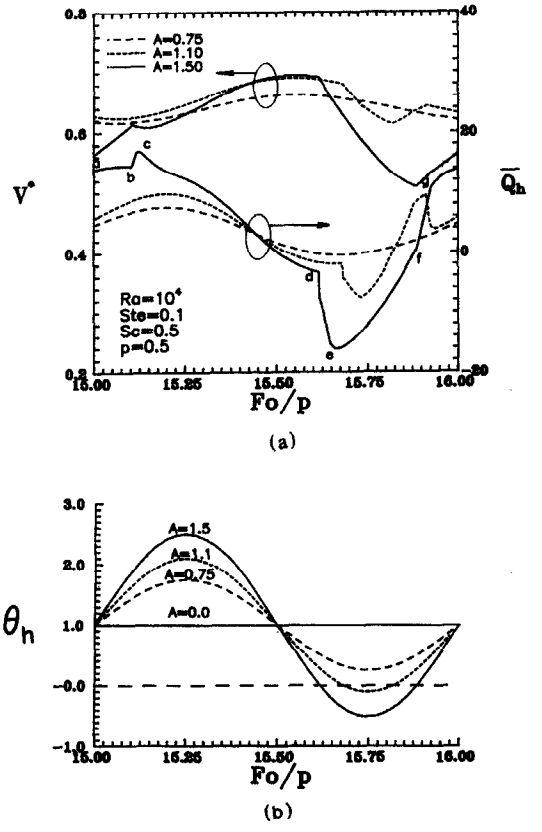

FIG. 4. Cyclic variation of (a) melting rate and average heat transfer rate at the hot wall, and (b) the imposed wall temperature.

assumed by $A = 0.75$, a periodic variation of V^* or $\bar{Q}_h$ with great complication arises for $A = 1.1$ and 1.5. The complicated cyclic behavior of $\bar{Q}_h$ for $A = 1.5$ in Fig. 4(a) can be characterized by several sub-intervals as denoted by the symbol sequence 'a'–'g'. The time interval 'a'–'b' represents an ongoing re-melting process of the re-frozen PCM next to the left wall. Such a re-melting process actually starts from the instant denoted by 'f' in the preceding cycle, thereafter the wall temperature re-rises above the PCM fusion point. During the interval 'b'–'c', $\bar{Q}_h$ is increased sharply up to a local maximum at the instant 'c'. This is due to intensified natural convection with continuously increasing hot-wall temperature, eventually leading to the occurrence of re-melting through the top portion of the re-frozen PCM layer sandwiched between two liquid PCM regions. Thereby, the natural convective flow in the re-molten PCM region adjacent to the left wall penetrates into the liquid PCM region next to the unmelted PCM attached to the fixed-temperature cold wall of the enclosure. Over the duration between 'c' and 'd', the heat transfer rate at the left wall, in accordance with the sinusoidal drop of the wall temperature, starts to decline quite monotonically and even becomes negative, that is a back heat flow out of the left wall of the enclosure. Further beyond the instant 'd', the left-wall temperature con-

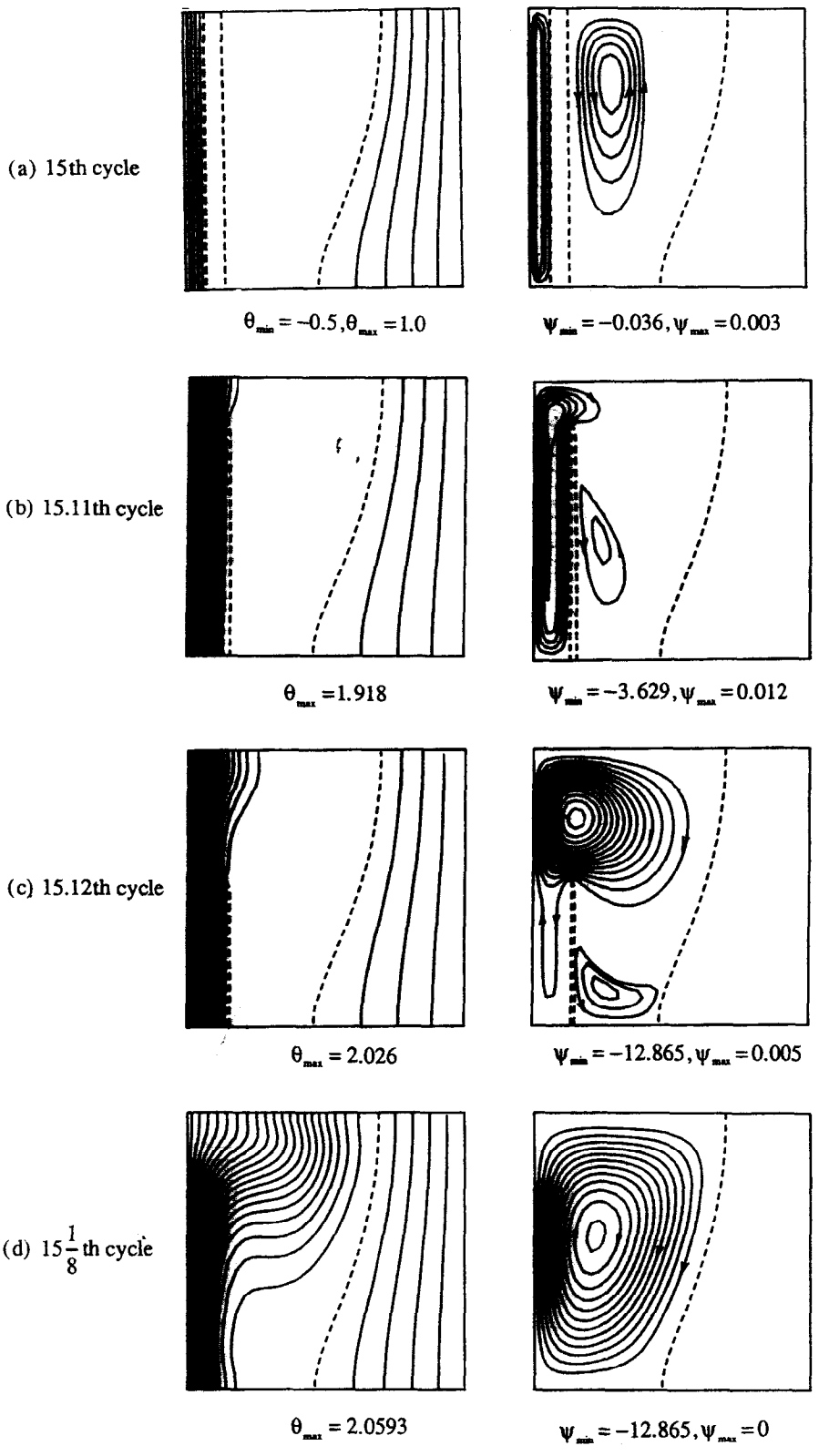

FIG. 5. Variation of flow structure and temperature distribution over a cycle of large-amplitude wall-temperature oscillations, $A = 1.5$ at $p = 0.5$ and $Ra = 10^4$.

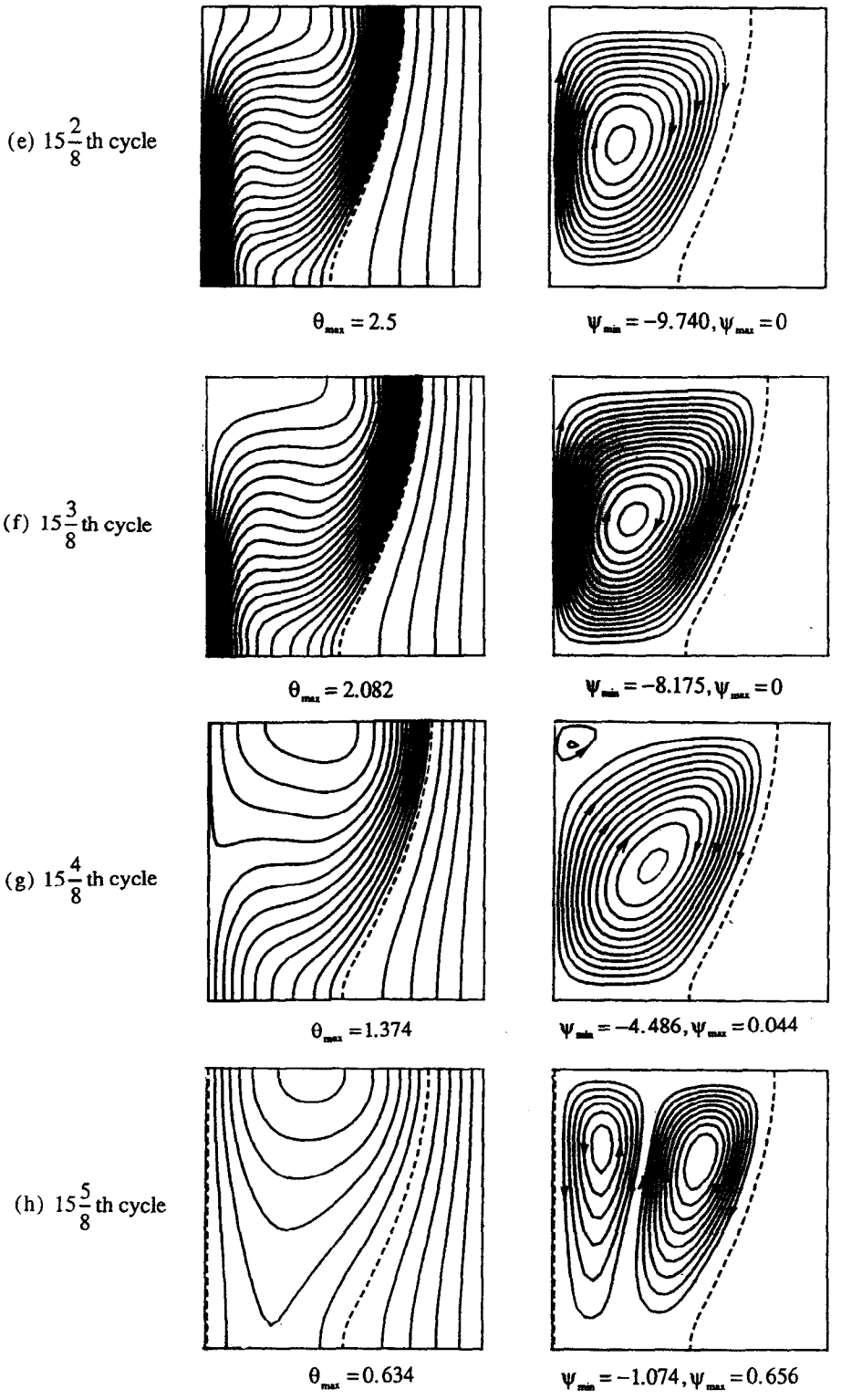

FIG. 5—*continued.*

tinues to fall below the PCM fusion point, whereby a re-solidification phenomenon of molten PCM occurs. Release of the latent heat accompanying the re-solidification phenomenon results in a precipitous increase of heat flux extracted out of the enclosure through the left wall. Similarly, the breaking of the smooth oscillatory variation of the average wall heat transfer rate can be readily detected for $A = 1.1$ in Fig. 4(a) when the decreasing wall-temperature curve crosses the fusion temperature of the PCM. During

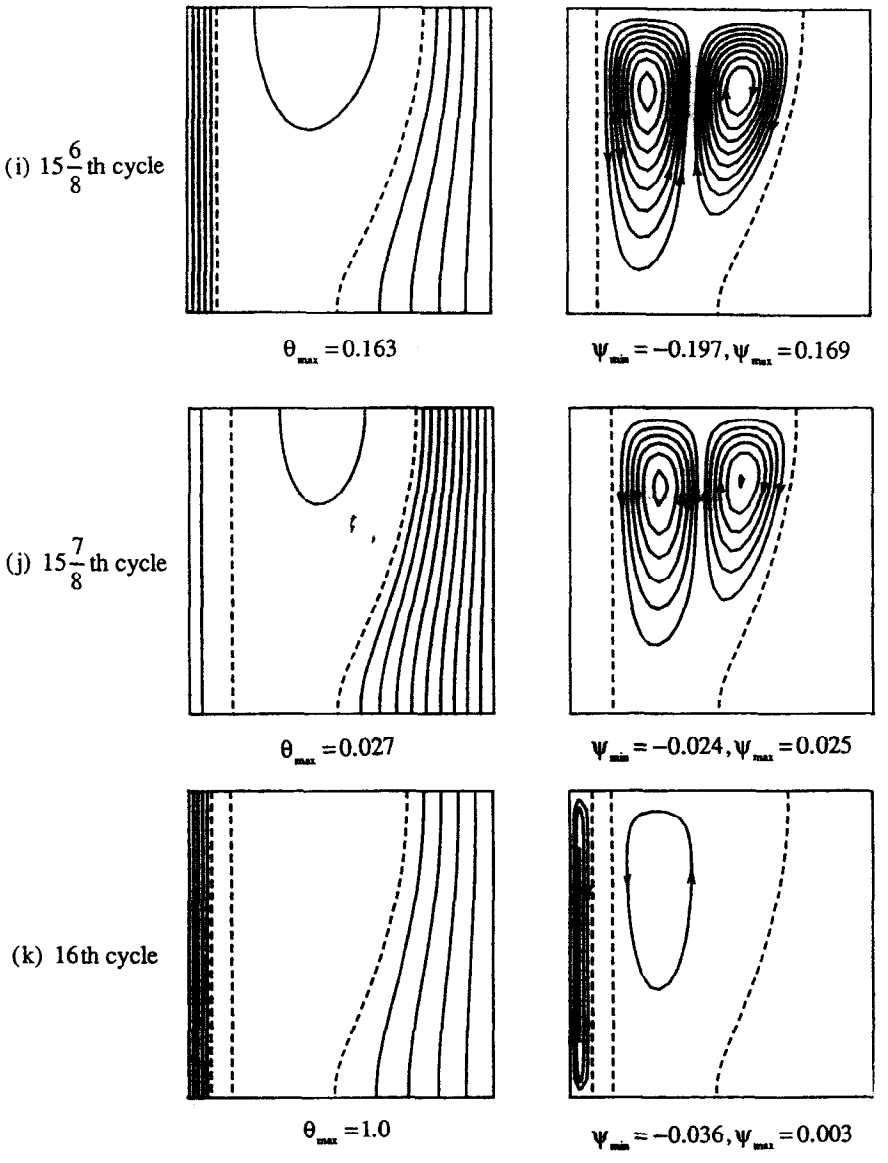

FIG. 5—*continued.*

the final quarter of the wall temperature cyclic oscillation, the negative heat transfer at the left wall gradually decreases until the onset of re-melting as a result of the wall temperature re-rising above the PCM fusion point; whence a positive heat transfer rate at the left wall resumes and becomes greatly enhanced as the re-molten PCM region is further expanded with time. Moreover, for the smaller wall-temperature perturbation amplitude $A = 1.1$, as shown in Fig. 4(a), the foregoing complicated variation of the melting rate and the heat transfer characteristics tends to be less distinctive. The above-elaborated complication of the periodic phase-change heat transfer behavior can be further inferred by examining the corresponding variation of the flow and temperature fields inside the enclosure as will next be discussed.

Figure 5 presents a sequence of contour plots of isotherms (left) and streamlines (right) for $A = 1.5$, $p = 0.5$, and $Ra = 10^4$ at different instants over the corresponding cycle of the wall-temperature oscillation shown in Fig. 4. In the contour plots, locations of the solid–liquid interfaces are denoted by dashed lines. At the beginning of the cycle, as clearly shown in Fig. 5(a), there coexist three solid–liquid interfaces with a solid PCM layer sandwiched between two molten PCM regions in addition to the unmelted PCM zone adjacent to the right cold wall of the enclosure. There exists a high temperature gradient across the enlarging re-melting layer next to the left wall, while a relatively isothermal condition prevails in the central molten region. In accordance with the continuing rise of the left-wall temperature, the clockwise recirculating flow in the re-melting layer greatly intensifies, hence resulting in a higher melting rate at the top portion of the re-frozen PCM layer. Consequently, as depicted in Fig. 5(b), the top portion of the sand-

wiched solid layer has already been melted through, and the clockwise circulation flow has extended across the tip of the re-frozen solid layer into the central molten region, suppressing the counter clockwise circulating flow there. After the one-eighth cycle of the wall-temperature oscillation, Fig. 5(d), the re-melting of the sandwiched solid layer has finished and the number of the moving boundaries reduces to one, having the clockwise recirculation as the dominating flow structure in the molten zone of the enclosure.

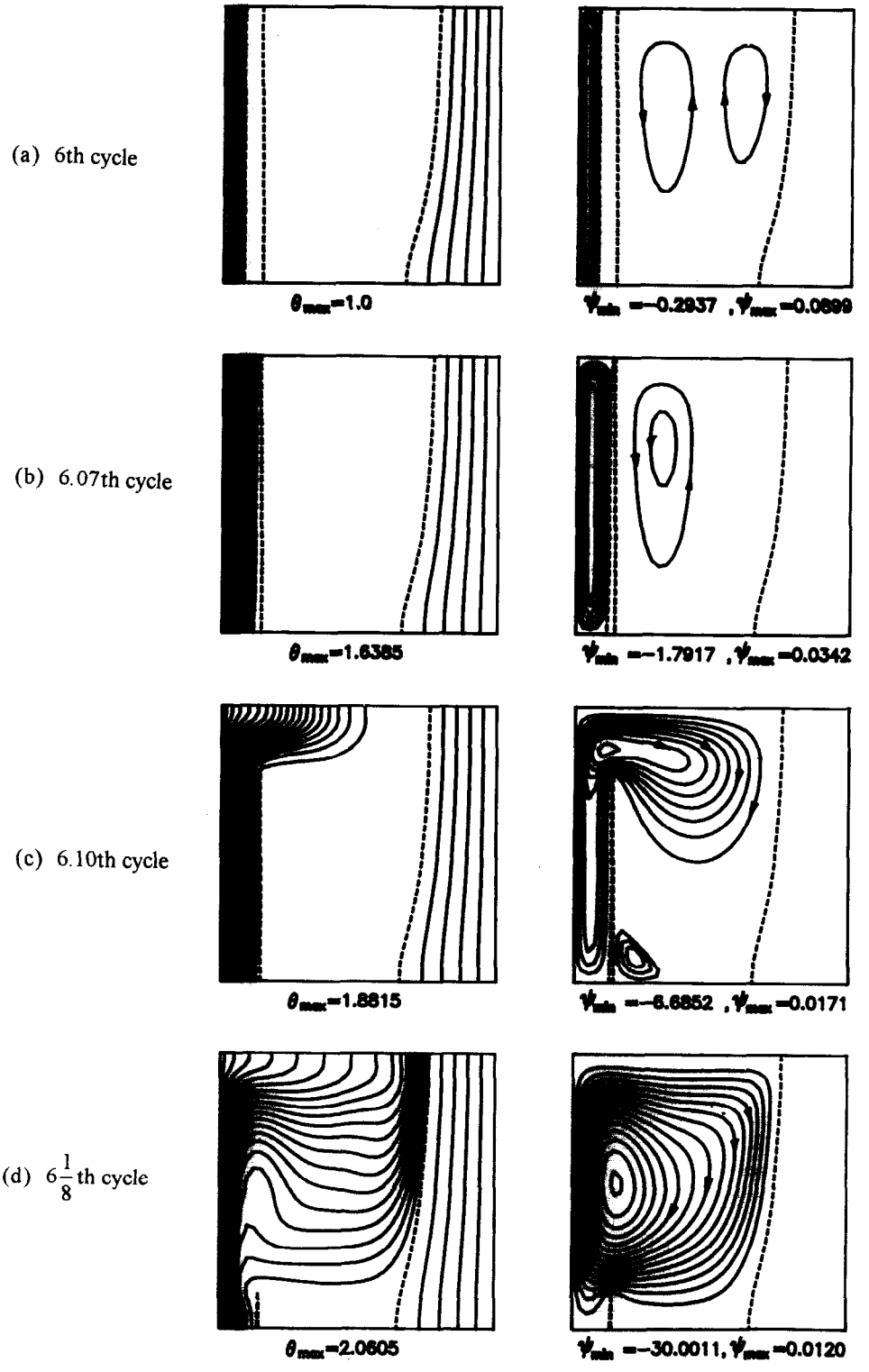

FIG. 6. Evolution of flow structure and temperature distribution over a cycle of large-amplitude wall temperature oscillations, $A = 1.5$ at $p = 0.5$ and $Ra = 10^5$.

Such an ordinary natural-convection-dominated melting pattern persists as the wall temperature continues to rise up to its maximum at the end of the first quarter cycle. Thereafter the left-wall temperature starts its sinusoidal drop; and the buoyant flow in the molten zone becomes subsequently impeded. Resembling the result found in ref. [5], at the end of the second quarter cycle a pocket of liquid PCM hotter than the left wall can be detected floating at the top region of the molten zone accompanied by the emerg-

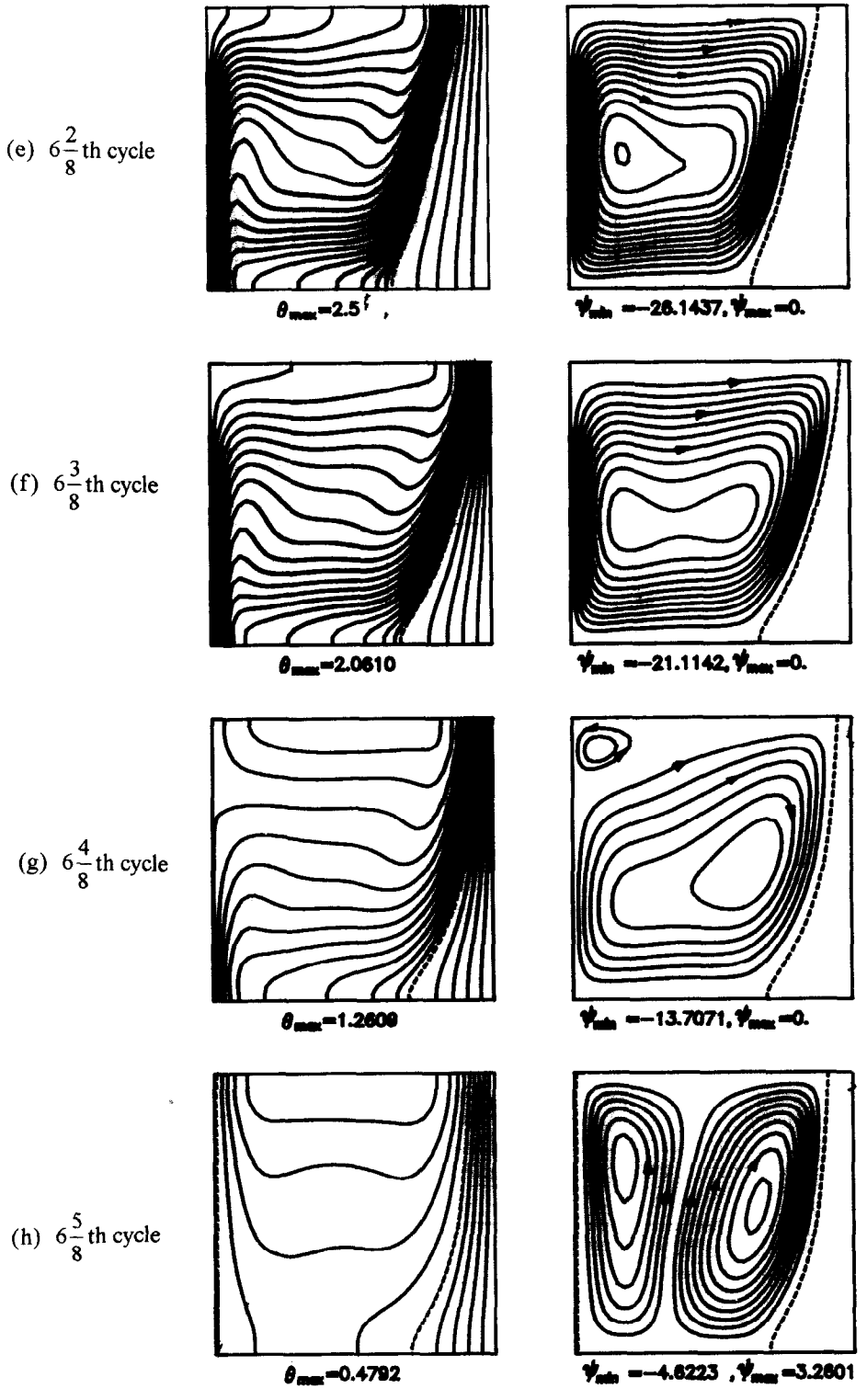

FIG. 6—*continued.*

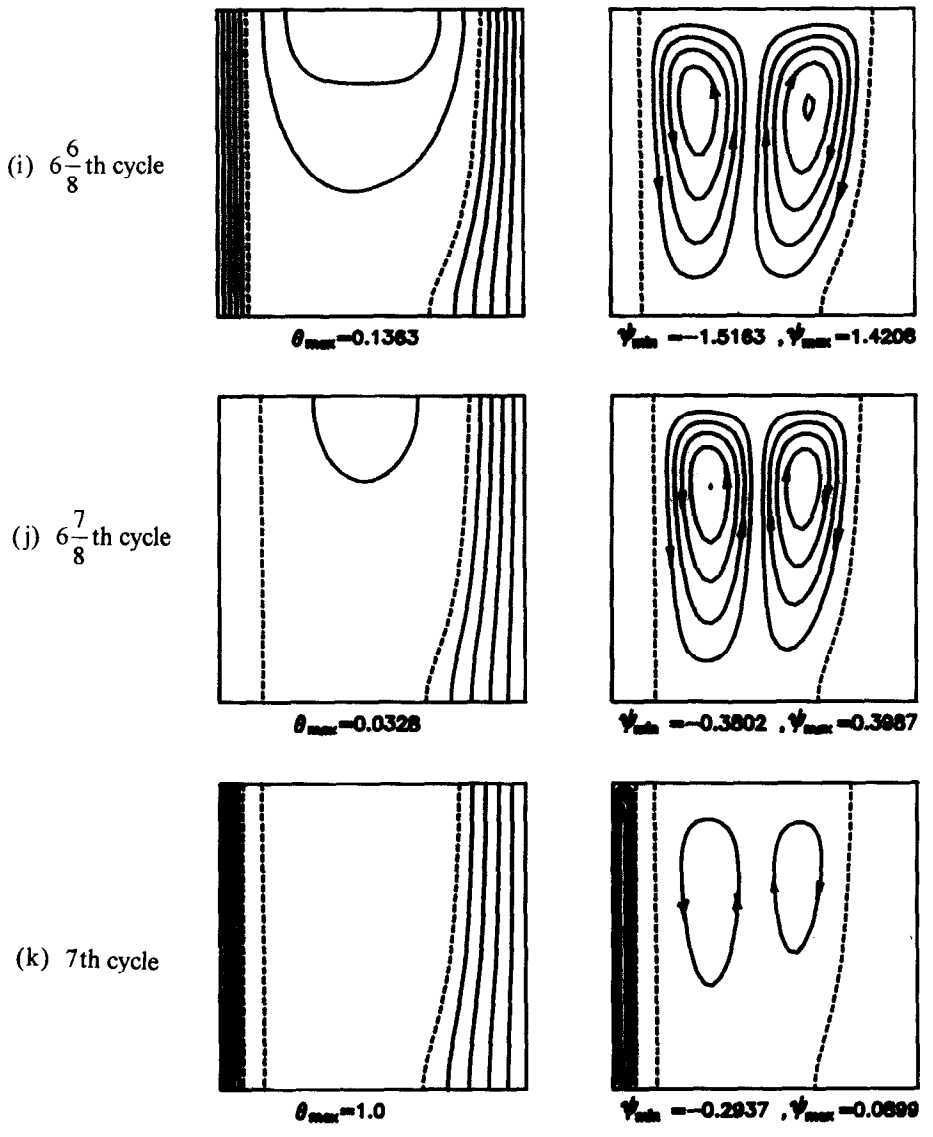

FIG. 6—*continued.*

ence of a counter-clockwise secondary eddy at the left top corner. Another result worth noticing is that the melting front still continues to move to the right even as the left-wall temperature declines through the second quarter cycle. The melting behavior at this stage is mainly driven by extraction of the sensible heat stored in the existent molten PCM region. Further proceeding into the third quarter cycle, as the left-wall temperature continues to fall further, the counter-clockwise circulation becomes progressively intensified and expanded, suppressing the clockwise flow. Consequently a bicellular flow structure prevails in the molten zone. Once the left-wall temperature drops below the PCM fusion point, a re-solidification process arises from the wall. As elucidated in Fig. 5(i), at the end of the third quarter cycle, a new solid–liquid interface emerges as a result of a re-frozen PCM layer formed at the left wall. The molten zone is accordingly reduced in size and appears to be somewhat isothermal as the clockwise recirculation next to the original melting front becomes gradually subdued. Over the final quarter cycle, the wall temperature rises, crossing the PCM fusion point, and the re-melting of the re-frozen PCM adjacent to the left wall takes place. The flow and temperature fields inside the PCM-filled enclosure evolve progressively back to those shown in Fig. 5(a). At a higher Rayleigh number, $Ra = 10^5$, the cyclic evolution of the temperature and flow fields as well as the solid–liquid interfaces inside the enclosure, as depicted in Fig. 6, exhibits characteristics similar to those above-elaborated for $Ra = 10^4$. As can be expected, the buoyancy-driven flow developed in the liquid regions is greatly enhanced at $Ra = 10^5$ as demonstrated by the higher extreme values of the stream function indicated in Fig. 6.

In Fig. 7 the influence of varying time period of the

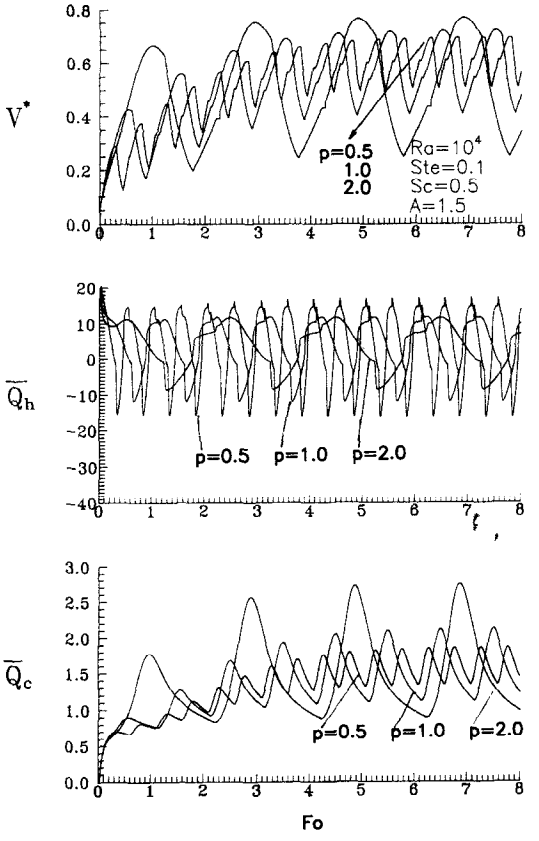

FIG. 7. Histories of melting rate and heat transfer rates under a fixed large-amplitude wall-temperature oscillation but with different time period.

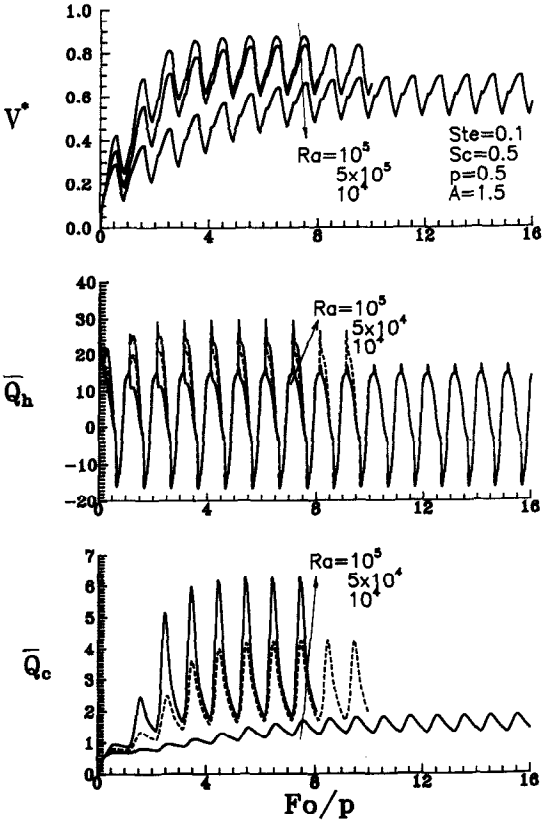

FIG. 8. Influence of Rayleigh number on the oscillatory melting rate and heat transfer rate under a large-amplitude cyclic wall-temperature condition.

imposed large-amplitude ($A = 1.5$) wall-temperature oscillation on the temporal variation of the melting rate and the average heat transfer rates at the vertical walls is conveyed. The effect of increasing the time period appears to be similar to the observations in refs. [5, 6], i.e. that a marked amplification of the induced steady oscillation amplitudes of both the melting rate and heat transfer rate at the cold wall arises, as can be seen in Fig. 7; while an adverse effect occurs for the heat transfer rate at the hot wall. This implies that the effect of varying time period on the melting rate and the heat transfer rate has little or no bearing on whether the imposed wall-temperature oscillation amplitude is greater than one or not.

Finally, the steady periodic melting behavior and heat transfer characteristics under the large-amplitude ($A = 1.5$) wall-temperature perturbation in Fig. 8 show a dependence on the Rayleigh number generally similar to that found for $A < 1$ [5, 6]. An increase of Rayleigh number tends to induce a higher-amplitude oscillation of the melting rate and the heat transfer rates at both vertical walls of the enclosure. Also as expected, the periodic mean values of the melting rate as well as the heat transfer rates at the vertical walls increase markedly with the increase of Rayleigh number.

CONCLUDING REMARKS

The main objective of the present paper is to present a numerical simulation of multiple solid–liquid interfaces arising in a natural-convection-dominated melting process inside a square enclosure imposed with time-periodic large-amplitude wall-temperature oscillation crossing the fusion point of the confined PCM. To effectively detect and treat the occurrence of the coexistent multiple moving boundaries, a solution algorithm developed in an earlier study [6] has been extended and demonstrated to be capable of solving the multiple phase fronts induced by the large-amplitude oscillatory wall-temperature condition on the PCM-filled enclosure. Considering *n*-octadecane as the PCM, parametric simulation has been performed mainly to illustrate the complicated solid–liquid phase-change phenomenon induced by the large-amplitude wall-temperature perturbation. As a result of the occurrence of re-solidification and then re-melting phenomena induced by the time-periodic wall-temperature oscillation through the PCM fusion point, there may coexist three solid–liquid interfaces inside the enclosure. Accordingly, the steady periodic phase-change heat transfer rate at the wall as well as the melting rate assume a very complicated cyclic variation in comparison with that found without the

occurrence of re-freezing and re-melting phenomena. The parametric simulation conducted here is certainly far from complete and further work will be carried out in the future. In addition, experimental work in this subject is needed for future studies.

REFERENCES

1. R. Viskanta, Phase-change heat transfer. In *Solar Heat and Storage: Latent Heat Materials* (Edited by G. A. Lane), pp. 153–222. CRC Press, Boca Rato, FL (1983).
2. R. Viskanta, Natural convection in melting and solidification. In *Natural Convection: Fundamentals and Applications* (Edited by S. Kakac *et al.*), pp. 845–877. Hemisphere, Washington, DC (1985).
3. R. Viskanta, Heat transfer during melting and solidification of metals, *J. Heat Transfer* **110,** 1205–1219 (1988).
4. S. Fukusako and N. Seki, Fundamental aspects of analytical and numerical methods on freezing and melting heat transfer problems. In *Annual Review of Numerical Fluid Mechanics and Heat Transfer*, Vol. 1 (Edited by T. C. Chawala), pp. 351–395. Hemisphere, New York (1987).
5. C. J. Ho and C. H. Chu, Periodic melting within a square enclosure with an oscillatory surface temperature, *Int. J. Heat Mass Transfer* **36,** 725–733 (1993).
6. C. J. Ho and C. H. Chu, The melting process of ice from a vertical wall with time-periodic temperature peturbation inside a rectangular enclosure, *Int. J. Heat Mass Transfer* **36,** 3171–3186 (1993).
7. C. Y. Choi and C. K. Hsieh, Solution of Stefan problems imposed with cyclic temperature and flux boundary conditions, *Int. J. Heat Mass Transfer* **35,** 1181–1195 (1992).
8. C. K. Hsieh and C. Y. Choi, Solution of one- and two-phase melting and solidification problems imposed with constant or time-variant temperature and flux boundary conditions, *J. Heat Transfer* **114,** 524–528 (1992).
9. P. J. Roache, *Computational Fluid Dynamics*. Hermosa, Albuquerque, NM (1976).